A Modular Framework for Shape and Image Prior Based Anatomical Structure Contour Extraction

Ayse Betul Oktay and Yusuf Sinan Akgul

GIT Vision Lab, http://vision.gyte.edu.tr/
Department of Computer Engineering, Gebze Institute of Technology, Gebze, Kocaeli 41400 Turkey

{oktay,akgul}@bilmuh.gyte.edu.tr

Running title: Prior Based Contour Extraction

Corresponding Author: Ayse Betul Oktay
E-mail: oktay@bilmuh.gyte.edu.tr
Phone +90 262 605 2230
Fax +90 262 605 2205

Abstract

Automatic extraction of anatomical structure contours from medical images is a challenging task in the presence of missing or unrelated parts, occlusions caused by other structures, and image noise. Employing prior information about the anatomical structures has been one of the most popular ways of addressing these challenges. This paper presents a novel framework that incorporates both shape and image priors into the contour extraction process with deformable contours. The framework handles the deformable contour evolution and the prior information integration separately by stopping the evolution of the deformable model and regularly re-initializing the expert contour with the most similar image and shape properties. The method can be used with any deformable model without complicating the deformable model functional. An explicit training phase is not required for the construction of the prior model. Moreover, it can be applied to any medical shape contour extraction task with simple modifications. The system is tested on echocardiographic images and cardiac MRI slices for the left ventricle border extraction under the level set framework. The visual and numerical results show the effectiveness of our method.

Keywords: Shape prior, Image prior, Deformable models, Level sets, Echocardiogram, Cardiac magnetic resonance image (MRI), Contour extraction

1. Introduction

Extraction of anatomical structure contours from medical images produces valuable information about the organ functions, organ structures, pathologies, etc., [1-3]. Manual extraction of the organ boundaries has a number of problems. First, the boundaries vary from expert to expert and subjective boundaries arise for the same organ [4]. Second, manual delineation process takes a huge amount of expert time, which is expensive. As a result, automatic extraction of the organ boundaries has been popular among the scientists to produce more accurate extraction results and fast consultation [5]. However, automatic extraction of the organ boundaries comes with its own difficulties. First, there may be unclear sections of the anatomical structures which are confusing for most of the methods. There might also be unrelated organ parts interfering with the structure of interest. Furthermore, there might be modality related issues such as signal drop-out and high amounts of speckle noise in ultrasound images. Therefore, the automatic extraction of anatomical structures is difficult as much as it is necessary.

Two classical contour extraction approaches in computer vision are snakes [6] and the level set method [7]. Although the snakes and level sets are powerful techniques, they cannot recover the structures in medical images accurately in most of the cases without prior knowledge due to the problems listed above. Incorporating prior knowledge about the target anatomical structure into the deformable contour evolution makes the contour extraction method consider not only the pixel-wise local image properties, but also the global properties. Therefore, incorporation of prior knowledge about the target anatomical structure is inevitable for the contour extraction.

There are several prior knowledge incorporation methods in the literature [8]. The active shape [9] and active appearance models (AAM) [10] are model-based object localization methods that use shape and appearance knowledge of the object for constraining the solution space. Leventon et al. [11] introduce prior information incorporation by using signed distance functions of the curves and principal component analysis (PCA) to form a statistical shape model from a training set. They embed an initial curve in the zero level of the surface which evolves towards maximum a posteriori estimate of the shape and pose. Chen et al. [12] use an average model as prior in its implicit function and they find the transformation of a given curve that projects it closer to the zero-level set of the implicit representation of the prior. Chen et al. [13] also use shape prior and intensity profile together for the extraction of contours in medical images. Tsai et al. [14] model the prior knowledge through a Gaussian distribution on the space of distance functions by performing singular value decomposition on a registered training set and recover the objects according to various data-driven terms. Rousson and Paragios [15] constrain the level set to follow a shape global consistency by creating a shape model with the Gaussian density function. The shape prior is imposed by the comparison between the model and the evolving contour. Wang et al. [16] add a new energy term to the main energy functional, so that global information is built into this function. Yan and Kassim [17] incorporate shape prior into the minimal path deformable model after defining mean and variance of the expert shapes with PCA.

The common prior incorporation technique in the approaches mentioned above is adding a new prior term into the deformable contour functional. Simultaneous incorporation of different types of prior knowledge, such as shape and image priors,

makes the functional more complicated and determining the optimal solution with many parameters like translation, rotation, and scaling becomes very hard [18]. Furthermore, constructing a training set and modeling variations of the target object within the training set are difficult. Instead of constructing a prior model by an explicit training phase and adding new terms into the deformable contour functional, we previously proposed a modular and flexible prior knowledge incorporation approach [19,20]. In that approach, the shape information is introduced to the contour extraction process by stopping the contour evolution and then regularly re-initializing the contour under the geometric effect of the most similar expert contour. Although the final extraction results are successful, the resulting contours do not localize some of the desired locations by using only geometric information.

In this paper, we propose a novel modular shape and image prior incorporation framework that can be used with deformable models like snakes and level sets in the light of our previous work. We employ image information besides the geometric information while re-initializing the contour. The expert contour that has the most similar geometric and image properties with the evolving contour is selected at regular intervals and that contour is re-initialized on the image after being warped onto the evolving contour.

The proposed method has several advantages. First, it is difficult to design a deformable model functional that incorporates complex shapes and their associated image properties. Our method follows a different approach and incorporates complex shape and image knowledge gathered from experts easily during re-initialization. Second, an explicit training phase is not required, so the prior information is incorporated directly during the contour evolution process. In addition, it is trivial to add new expert

knowledge to the system on the fly due to the lack of an explicit training phase. Finally, the system can be used with any deformable model without increasing the computational power requirements significantly.

The developed framework is tested on echocardiograms and cardiac MRIs to extract left ventricle boundaries (Figure 1). The test images have different characteristics and there are many modality and organ related difficulties for the contour extraction. The echocardiographic images are the short-axis transthoracic views of the left ventricle which include high amounts of noise and unclear cardiac wall parts. The 2D cardiac MRI slices are end-diastolic short-axis views of the heart. Although they are not as noisy as echocardiograms, they include unrelated high contrast structures like papillary muscles around the cardiac wall.

The rest of this paper is organized as follows: The contour extraction framework with the shape and image priors is introduced in Section 2. Extraction of the left ventricle borders with the level set method is presented in Section 3. Section 4 includes the experimental results. Finally, we conclude in Section 5.

2. Method: prior based contour extraction framework

Our method of incorporating the prior knowledge consists of two repeating stages. In Stage I, the deformable model evolves according to the classical formulation without prior information. Stage II selects one of the expert contours according to shape and image similarity measure and re-initializes that contour on the image after a transformation for further evolution. Then Stage I starts again, which is followed by Stage II, until the deformations stop. An overview of the system is shown in Figure 2.

2.1.The shape prior

Anatomical structures have similar shape and geometric properties, so the expected final extraction of the deformable model should have such a shape. While the deformable model evolves without prior knowledge in Stage I, there may be undesirable deformations caused by the structure of other organs and image artifacts. Incorporating the knowledge of target structure's geometry prevents such undesirable deformations by guiding the deformable model towards specific shapes.

Consider a discretized closed contour as $C = \{c_1, \ldots, c_n\}$ consisting of n ordered 2D points evolving in Stage I. The continuous contour C can be recovered by interpolating these points. Let $E = \{E_1, \ldots, E_k\}$ be a set of k discretized expert contours where $E_i = \{e_1, \ldots, e_m\}$ is represented by ordered 2D m points. Our shape prior method requires finding the expert contour E_i where the similarity between C and E_i is highest. Unfortunately, the shape similarities between the expert contours and the evolving contour C cannot be found directly because of the scale, translation, rotation, and local geometric shape differences. However, by taking advantage of the nature of the organ shapes, practical deformable contour matching algorithms can be used to find the shape similarity.

In our deformable matching method for the left ventricle contours, we first find the center of mass positions of the contour C and each of the expert contours in the set E. The center of mass positions are translated to $(0,0)$ point in the Cartesian system. The function $R(c_i)$ defines the Euclidian distance between the contour position c_i and

the origin $(0,0)$. The function $\theta(c_i)$ defines the angle between x axis and the line passing through point $(0,0)$ and point c_i (Figure 3).

We rotate the expert contours in order to handle the orientational differences between the expert contours and the evolving contour. We create a new set E^r from the expert contour set E by rotating each E_i in a narrow angle range by small increments. Note that, the set E^r contains many rotated forms for each element of E.

In order to measure the similarity between the evolving contour $C = \{c_1, \ldots, c_n\}$ and a rotated expert contour $E_i^r = \{e_1^r, \ldots, e_m^r\}$, we find a local scaling amount for each point e_j^r and c_i by using h ordered neighboring points around c_i where $\theta(c_i) \cong \theta(e_j^r)$. We calculate the warped point e_j^w by

$$e_j^w = \frac{\sum_{p=-h/2}^{h/2} R(c_{i+p})}{\sum_{p=-h/2}^{h/2} R(e_{j+p}^r)} R(e_j^r). \quad (1)$$

All points of the rotated contour $E_i^r = \{e_1^r, \ldots, e_m^r\}$ are warped onto the evolving contour C and we get the new warped expert contour $E_i^w = \{e_1^w, \ldots, e_m^w\}$ with Eq. (1). All of the rotated expert contours in set E^r are warped to C and a new warped contour set E^w is constructed.

The geometric similarity G of a warped expert contour $E_i^w = \{e_1^w, \ldots, e_m^w\}$ with $C = \{c_1, \ldots, c_n\}$ is defined as

$$G(C, E_i^w) = \sum_{i=1}^{n} \left| c_i - e_j^w \right|, \quad (2)$$

where $\theta(c_i) \cong \theta(e_j)$.

After determining the shape similarity of each expert contour with Eq. (2), we also find their image similarities with the evolving contour for selecting the expert contour that will be re-initialized. The calculation of the image similarity is explained in the next section.

2.2. The image prior

Choosing the expert contour only according to the geometric similarity may sometimes cause inaccurate localizations of the evolving contour. While the contour evolves in Stage I, it may be affected by low or high contrast image parts around the organ and may not reach to the organ boundaries. If only the shape prior is employed in Stage II, the contour might have a similar shape with the prior, but it may not localize accurately around the boundary of the target organ. We argue that not only the geometric properties but also the image properties around the organ boundaries must be similar. Therefore, we employ a similarity metric that combines the image similarity with the shape similarity between the evolving and expert contours.

The image similarity N between the evolving contour C on image I_c and an expert contour E_i delineated for image I_e is found by summing the normalized cross correlation (*NCC*) values in patches around the corresponding points. Consider $p(I, s)$ as a function that returns the image patch around point s in image I and *NCC* as the normalized cross correlation function. The image similarity $N(C, E_i)$ between the evolving contour $C = \{c_1, \ldots, c_n\}$ and an expert contour $E_i = \{e_1, \ldots, e_m\}$ is defined by

$$N(C, E_i) = \sum_{k=1}^{n} NCC(p(I_c, c_k), p(I_e, e_j)), \quad (3)$$

where $\theta(c_i) \cong \theta(e_j)$ which means that c_i and e_j are corresponding points.

Each expert contour has geometric similarity and image similarity values with the evolving contour C determined by Eq. (2) and Eq. (3), respectively. An expert contour $E_i \in E^w$ that has the maximum combined image and geometric similarity value is determined by

$$\arg\max_{E_i \in E^w} \{\alpha_t N(C, E_i) - (1-\alpha_t) G(C, E_i^w)\}, \quad (4)$$

where $0 < \alpha_t < 1$ is a weighting constant that linearly increases its value with iteration number t of the repeating Stages I and II (Figure 2). At the initial iterations, the value of α_t is selected close to zero which makes the prior selection biased towards the shape prior term. This is useful to enforce a shape similarity at the initial deformation stages so that unrelated image features would not affect the final results. When the evolving curve approaches near the organ boundaries during later iterations, α_t becomes larger and gives more weight to the image information of the expert contours.

3. Contour extraction with priors

Although our formulation for prior incorporation uses level sets, our method can be easily extended to other deformable models. We use the variational level set formulation [21] due to its advantages of easy implementation and computational efficiency.

Extraction of the inner and outer left ventricle borders (endocardium and epicardium shown in Figure 1 (a) and (b)) can be done at the same time, so we use a

coupled contour evolution process where the contours evolve in a way that they try to move smoothly towards each other.

Let $f_1(t)$ and $f_2(t)$ be time t dependent closed concentric curves evolving on the plane $\Re^2$ for extracting the endocardium and epicardium, respectively. Consider F as the set of points on $f_1(0)$ and $f_2(0)$ at $t=0$ and $\mathbf{x} \in \Re^2$ as the position vector. The discretized signed distance function $\phi : \Re^2 \to \Re$ is defined as

$$\phi(\mathbf{x}) = \begin{cases} 0, & \text{if } \mathbf{x} \in F \\ -d(\mathbf{x}, F), & \text{if } \mathbf{x} \text{ is outside } f_1 \text{ but inside } f_2 \\ d(\mathbf{x}, F), & \text{otherwise,} \end{cases} \tag{5}$$

where $d(\mathbf{x}, F)$ is the shortest Euclidian distance to F from point $\mathbf{x}$. The contours f_1 and f_2 are the zero level set of ϕ at $t=0$.

The 3D surface ϕ evolves under the influence of the internal energy term $P(\phi)$ and the external energy term $\varepsilon_m(\phi)$. The variational energy functional $\varepsilon(\phi)$ is defined as:

$$\varepsilon(\phi) = \mu P(\phi) + \varepsilon_m(\phi), \tag{6}$$

where μ is a parameter controlling the weight of the internal energy term in the overall contour extraction process. The internal energy term forces the level set functional not to deviate from the signed distance function which is desired to satisfy $|\nabla\phi| = 1$. The external energy term moves the zero level of the surface towards the object boundaries. The details of the level set formulation can be found in [21].

We initially construct a discretized surface ϕ with Eq. (5) by placing a zero level contour f_1 inside endocardium and a zero level contour f_2 outside epicardium on an image. In Stage I, the surface ϕ evolves under the influence of the internal and external

energy terms. It is expected that the zero level contours f_1 and f_2 move towards each other for some time under the image forces. At regular intervals the evolution is stopped and the most similar expert contour is selected by Eq. (4) in Stage II for the endocardium and epicardium separately. A new surface is constructed by Eq. (5) by embedding the selected warped expert contours at the zero level. The new surface is re-initialized on the image and it continues to evolve in Stage I. Stage I and II follow each other until the whole process converges to the final result. The flow of the method is shown in Algorithm 1 and Figure 2. The running time of the algorithm depends on iteration count T, number of expert contours k, re-initialization interval r, and the matching method used.

Algorithm 1 Contour extraction with prior based level set method

Input: Expert contours E=$\{E_1,\ldots,E_k\}$, T iteration count, r re-initialization interval, image I

Output: The zero level set of final surface ϕ

Require: Construct an initial 3D surface ϕ by Eq. 5

for $t=1$ to T **do**

Evolve ϕ with Eq. 6

if mod(t, r)==0 **then**

Get zero level set c of ϕ

Rotate and scale expert contours with Eq. 1 and get warped contour set E^w

Use Eq. 4 to find the expert contour which is most similar to c

Use Eq. 5 to create new 3D surface ϕ from the most similar expert contour

Re-initialize ϕ on the image

end if

end for

4. Experimental results

This section describes the numerical comparisons and shows the visual results of the contour extraction experiment from the echocardiographic images and 2D cardiac MRI slices.

4.1.Contour extraction from echocardiograms

The echocardiographic images used in this study are left ventricular short axis transthoracic views during the cardiac cycle. They are very noisy and there are low contrast parts around the cardiac borders. There are total of 28 echocardiographic images from 28 different people which are 250 by 200 pixels in size. The data is gathered from both healthy and unhealthy subjects. We use 8 of the 28 echocardiographic images for the geometric and image priors and we tested the system on the remaining 20

echocardiographic images. The epicardium and endocardium contours for each image in the data set are traced by four different experts (Exp1, Exp2, Exp3, Exp4) independently. The numerical values of the system parameters are selected as follows: the internal energy term μ is 0.04, the re-initialization interval r is 15, the iteration count T is 150, and the number of neighboring points h in Eq. 1 is 6.

For each image, we automatically produce three different contours. First one is produced by the method that uses only shape prior [20]. In other words, [20] selects α_t of Eq. 4 as 0 for all iterations. The second contour produced by our method uses both shape and image priors together. The third contour is produced by the level set method without prior information [21]. During the evolution process, the level set front may leak from the gaps caused by signal dropout and change topology in the lack of priors. We stopped the surface evolution to prevent the topology change when two contours get close to each other less than 2 pixels.

We numerically compare the automatically detected contours with the expert delineations of 20 images. The delineations of the experts are also compared with each other to obtain the variation between the experts. Given two contours $C_x = \{x_1, ..., x_n\}$ and $C_y = \{y_1, ..., y_m\}$, the average pixel difference between the contours is calculated by

$$PD(C_x, C_y) = \frac{\sum_{i=1}^{n} d(x_i, C_y) + \sum_{j=1}^{m} d(y_j, C_x)}{n+m}, \quad (7)$$

where $d(x, C)$ is the minimum Euclidean distance between the 2D point x and the contour C.

The contours for the same image are compared with each other using Eq. 7. The averages of the comparisons for 20 images are reported in Table 1. Figure 4 includes

three of the test images with the expert and automatically detected contours. The analysis of the numerical values and visual inspection of the results indicate that automatically detected contours by our method are within the inter-expert variations. In other words, the comparison values between the human experts are not distinguishable from the comparison values between the experts and automatically detected contours of our method. On the other hand, the results of the level set method without prior information [21] have high differences with the experts.

Our method has less pixel difference than [20] by an approximate quarter of a pixel. In order to determine the statistical significance between our method and [20], we perform a one-tailed, paired t-test [23] with the average differences with experts. A *p* value of less than 0.05 implies the statistical significance. We get *p* value less than 0.05 which shows that the difference between our method and [20] is statistically significant. Therefore, employing both geometric and image prior information produces better extraction results.

The expert contours used as prior should be chosen as representative samples and all shape possibilities must be covered. There is not much variance between the organ shapes for our application, so a small number of expert contours are sufficient to describe the organ geometry. For the left ventricle shapes in our dataset, we determined that 8 expert contours are sufficient. However for more complex organ shapes, more expert contours must be used. In order to show the effect of selected priors on the contour extraction process, we ran the system on the same image with five different expert contour sets as priors where each set includes 8 different expert contours for a total of 200 iterations (T = 200). The re-initialization interval is selected as 15 iterations (r=15).

We measured the comparison value between the current evolving contour and the expert contour after every 10^{th} iteration. Figure 5 shows the pixel differences during the system iterations. The system reaches the same pixel difference values (about 3 pixels) regardless of the prior expert contour set used. As a result, our system results are not biased towards a specific expert contour because changing the expert contours would not degrade the system performance. Figure 5 also shows the effects of using prior information in the extraction process. If the system does not use any priors, the pixel difference between the resulting contour and the expert contour becomes very large (around 9 pixels), which indicates the significance of the prior information. Figure 5 also shows the numerical stability of our system. The iterations always lower the pixel errors and it reaches the convergence after some fixed number of iterations.

4.2.Contour extraction from cardiac MRIs

We also applied our method to cardiac MRIs that contain unrelated high contrast parts around the cardiac borders. The cardiac MRI dataset [22] includes 14 2D cardiac MRIs from healthy people which are 256 by 256 pixels in size. All images are short-axis, end-diastolic cardiac MRIs, acquired using a whole-body MR unit operating at 1.0 Tesla. The endocardial and epicardial contours of the left ventricle are annotated manually by placing 33 landmarks along each contour by an expert. The numerical values of the system parameters are same with the previous experiment except the number of neighboring points h. In this experiment, the value of h is selected as 4 instead of 6 because the total number of landmark points in MRIs are less than the total number of landmark points in echocardiograms.

The validation of our method is performed using leave-one-out evaluation. In order to compare our results with active appearance model results in [22], we calculated point to curve error which is defined as

$$D(\mathbf{x}_{ec}, \mathbf{x}) = \frac{1}{n}\sum_{i=1}^{n} \min_{t} \sqrt{(x_i - r_y(t))^2 + (y_i - r_x(t))^2}, \quad (8)$$

where $r(t) = (r_x(t), r_y(t)),\ t \in [0,1]$ is the linear spline fitted to the expert contour (ec) landmark points and $\mathbf{x}$ includes the points of extracted contour.

The contour extraction results of our system and the methods of [22] are shown in Table 2. [22] applied the basic AAM and three extensions to AAM - which are inferring knowledge from the pixel neighborhood, model fitting by simulated annealing, and using Lorentzian distance as the error norm - and the experiments are conducted by leave-one-out approach on the same dataset. The minimum error of [22] is 1.06 pixels. The point to curve error of our extraction is 1.02 pixels. Figure 6 shows our extraction results and the expert delineated contours for all images in the dataset. The visual inspection of our extraction results shows that our system is also very robust on cardiac MRIs.

5. Discussion and conclusions

We have introduced a modular prior knowledge integration framework for the deformable models to extract the anatomical structure contours in medical images. The developed framework regularly re-initializes the evolving contour by selecting one of the expert contours according to shape and image similarities.

The modularity of the developed method provides a flexible environment for the contour extraction. First, it can be used efficiently with the methods like snakes and level sets. Second, it can be applied to many anatomical structures by changing the process of

selecting the most similar expert contour, i.e., the contour matching method. Although we have used a trivial matching method in this study, more efficient and faster matching methods can be incorporated into the system.

Our approach differs from the classical prior-based contour extraction methods in that there is no initially defined prior model created by explicit training. Instead, the prior knowledge is employed directly during the model deformations by re-initialization. This brings the advantage of adding and removing new expert knowledge on the fly without the risk of overtraining. Also, it facilitates a more convenient way of debugging the system. There may be nonrepresentative expert contours which show considerable variations from the expected shape contours. Any nonrepresentative contour that causes a problem can be found immediately. Although we have used shape and image knowledge in order to select the expert contour, other knowledge can be incorporated easily into this selection process. For example, hard constraints, such as number of corners and the inner contour area can be enforced during the contour re-initialization. Another important aspect of the developed method is that the prior terms are not included in the deformable model functional. The separation of the contour evolution and prior information integration results in a simpler, more modular, and more flexible formulation. Moreover, the scale, rotation, and translation problems are resolved in the process of matching the expert contours and they are not included in the deformable model functional.

The classical prior based contour extraction methods usually assume a distribution for the expected shapes. These methods need to know the distribution type and the distribution parameters have to be estimated, which requires careful selection of representative samples from the shape domain. Although our method also needs

representative samples, it does not assume a distribution and there are no parameter estimation phases.

In spite of many advantages, there are a few issues in our system. First, the system cannot detect open contours and multiple intersecting objects without using complicated contour matching methods. Second, the alternative classical methods can handle a few nonrepresentative contours during training; however our system may not tolerate any nonrepresentative contours in case these contours are selected during the re-initialization phase. Another drawback is the increased computation time with the increasing number of prior shapes. However, the computation time can be decreased by using faster matching algorithms.

Acknowledgments

We would like to thank Jens Chr. Nilsson and Bjorn A. Gronning for the cardiac MRI data set and University of Washington's Echocardiographic Laboratory for the echocardiographic images.

References

[1] D. P. Mukherjee, N. Ray and S. T. Acton, "Level set analysis for leukocyte detection and tracking," *IEEE Trans. Image Process*., 13: 562-572, 2004.

[2] J. M. B. Dias and J. M. N. Leitao, "Wall position and thickness estimation from sequences of echocardiographic images," *IEEE Trans. Med. Imaging*, 15: 25-38, 1996.

[3] G. Jacob, J. A. Noble, C. Behrenbruch, A. D. Kelion and A. P. Banning, "A shape-space-based approach to tracking myocardial borders and quantifying regional left-ventricular function applied in echocardiography," *IEEE Trans. Med. Imaging*, 21: 226-238, 2002.

[4] H. Lee, N. C. F. Codella, M. D. Cham, J. W. Weinsaft and Yi Wang, "Automatic left ventricle segmentation using iterative thresholding and an active contour model with adaptation on short-axis cardiac MRI," *IEEE Trans. Biomed. Eng.*, 57: 905-913, 2010.

[5] L. Grady, "Random walks for image segmentation," *IEEE Trans. Pattern Anal. Mach. Intell*., 28: 1-17, 2006.

[6] M. Kass, A. Witkin and D. Terzopoulos, "Snakes: active contour models," *Int. J. Comput. Vision,* 1: 321-331, 1987.

[7] S. Osher and J. A. Sethian, "Fronts propagating with curvature dependent speed: algorithms based on hamilton-jacobi formulation," *J. Comput. Phys.,* 79: 12-49, 1988.

[8] D. Cremers, M. Rousson and R. Deriche, "A review of statistical approaches to level set segmentation: integrating color, texture, motion and shape," *Int. J. Comput. Vision*, 72: 195-215, 2007.

[9] T. F. Cootes, C. J. Taylor, D. H. Cooper and J. Graham, "Active shape models-their training and application," *Comput. Vision Image Understanding*, 61: 38-59, 1995.

[10] T. F. Cootes, G. J. Edwards and C. J. Taylor, "Active appearance models," *Proc. Eur. Conf. Comput. Vision,* 2: 484-498, 1998.

[11] M. Leventon, E. Grimson and O. Faugeras, "Statistical shape influence in geodesic active contours," *Proc. IEEE Conf. Comput. Vis. Pattern Recognit.*, 316-322, 2000.

[12] Y. Chen, H. Thiruvenkadam, H. Tagare, F. Huang and D. Wilson, "On the incorporation of shape priors into geometric active contours," *Proc. IEEE*

Workshop on Variational and Level Set Methods in Comput. Vision, 145-152, 2001.

[13] Y. Chen, F. Huang, H. D. Tagare and M. Rao, "A coupled minimization problem for medical image segmentation with priors," *Int. J. Comput. Vision*, 71: 259-272, 2006.

[14] A. Tsai, A. Yezzi, W. Wells, C. Tempany, D. Tucker, A. Fan, E. Grimson and A. Willsky, "Model-based curve evolution technique for image segmentation," *Proc. IEEE Conf. Comput. Vision Pattern Recognit*., 463-468, 2001.

[15] M. Rousson and N. Paragios, "Shape priors for level set representations," *Proc. Eur. Conf. Comput. Vision*, 78-92, 2002.

[16] Y. Wang and L. H. Staib, "Boundary finding with prior shape and smoothness models," *IEEE Trans. Pattern Anal. Mach. Intell*., 22: 738-743, 2000.

[17] P. Yan and A. A. Kassim, "Medical image segmentation using minimal path deformable models with implicit shape priors," *IEEE Trans. Inf. Technol. Biomed.*, 10: 677-684, 2006.

[18] A. Besbes, N. Komodakis, G. Langs and N. Paragios, "Shape priors and discrete MRFs for knowledge-based segmentation," *Proc. IEEE Conf. Comput. Vision Pattern Recognit.,* 1295-1302, 2009.

[19] A. B. Oktay and Y. S. Akgul, "A novel level set based echocardiographic contour extraction method with prior knowledge," *Proc. Br. Mach. Vision Conf.*, 975-984, 2008.

[20] A. B. Oktay and Y. S. Akgul, "Prior information based segmentation: a 3D level set surface matching approach," *Proc. Int. Symposium on Comput. and Information Sciences,* 2008.

[21] C. Li, C. Xu, C. Gui and M. D. Fox, "Level set evolution without reinitialization: a new variational formulation," *Proc. IEEE Conf. Comput. Vision Pattern Recognit.,* 430-436, 2005.

[22] M. B. Stegmann, "Active appearance models: Theory, extensions and cases," M. Eng. thesis, Informatics and Mathematical Modelling, Technical University of Denmark, Lyngby, 2000, available online: http://www.imm.dtu.dk/~aam/.

[23] M. J. Graves, E. Berry, A. Avedisijan, M. Westhead, R. T. Black, D. J. Beacock, S. Kelly and P. Niemi, "A multicenter validation of an active contour-based left ventricular analysis technique," *J. Magn. Reson. Imaging,* 12: 232-239, 2000.

Table 1 The differences (in pixels) of our method, [20], [21] and expert detected contours.

	Exp 2	**Exp 3**	**Exp 4**	**Only shape prior[20]**	**Li et al. [21]**	**Our method**
Exp 1	3.33	3.10	5.65	4.12	7.19	3.80
Exp 2		3.26	5.59	4.77	7.82	4.46
Exp 3			5.33	4.94	7.38	4.76
Exp 4				5.33	8.40	5.06

Table 2 The point to curve errors (in pixels) on the cardiac MRI dataset.

Method	**Error**
Our method	1.02
Basic AAM [22]	1.18
Neighborhood [22]	1.73
Simulated Annealing [22]	1.06
Lorentzian [22]	1.13

Figure 1 An example (a) echocardiographic image and (b) a cardiac MRI slice where the inner and outer cardiac borders are marked by an expert.

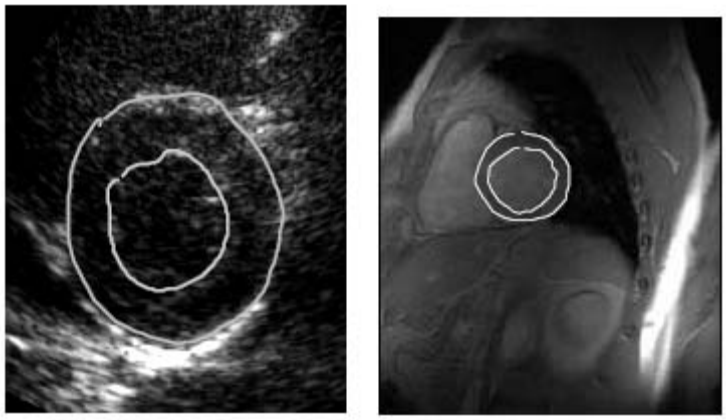

(a) **(b)**

Figure 2 An overview of the developed system.

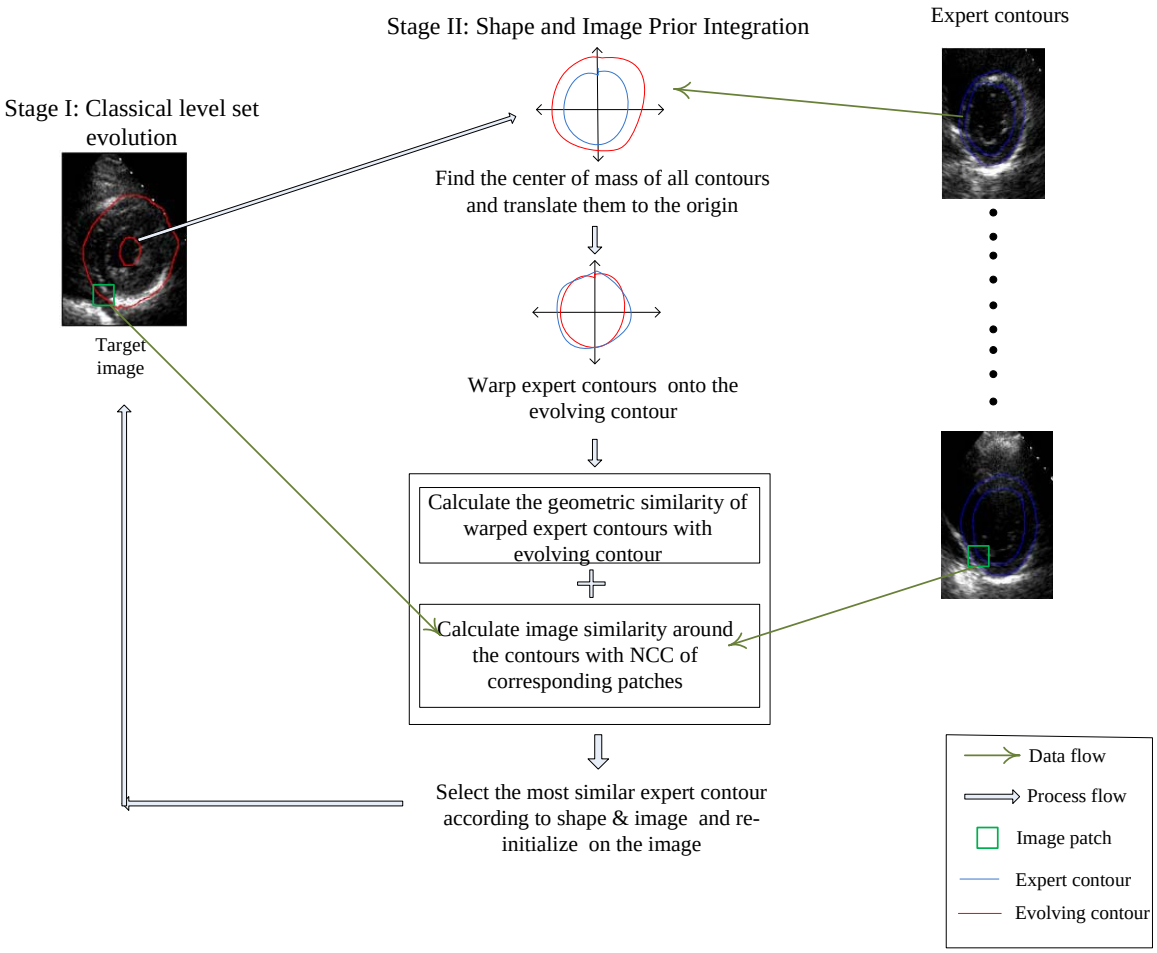

Figure 3 An example point c_i, $\theta(c_i)$ and $R(c_i)$ in 2D Cartesian coordinate system.

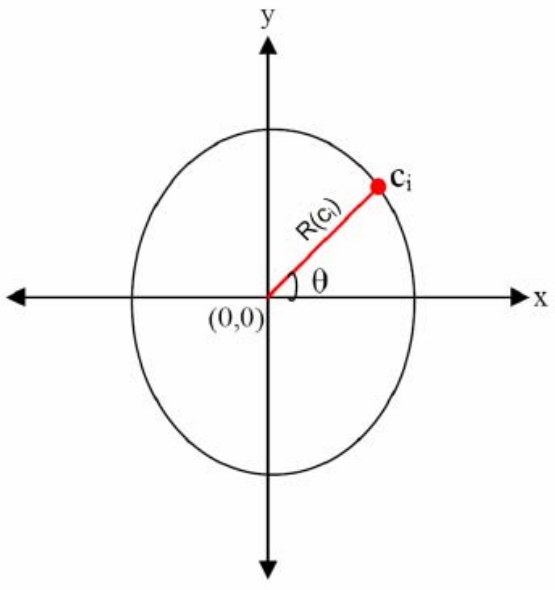

Figure 4 (a) Echocardiographic images. (b) Automatically detected contours by the developed method (Auto2) are shown in red and the expert contours are shown in yellow.

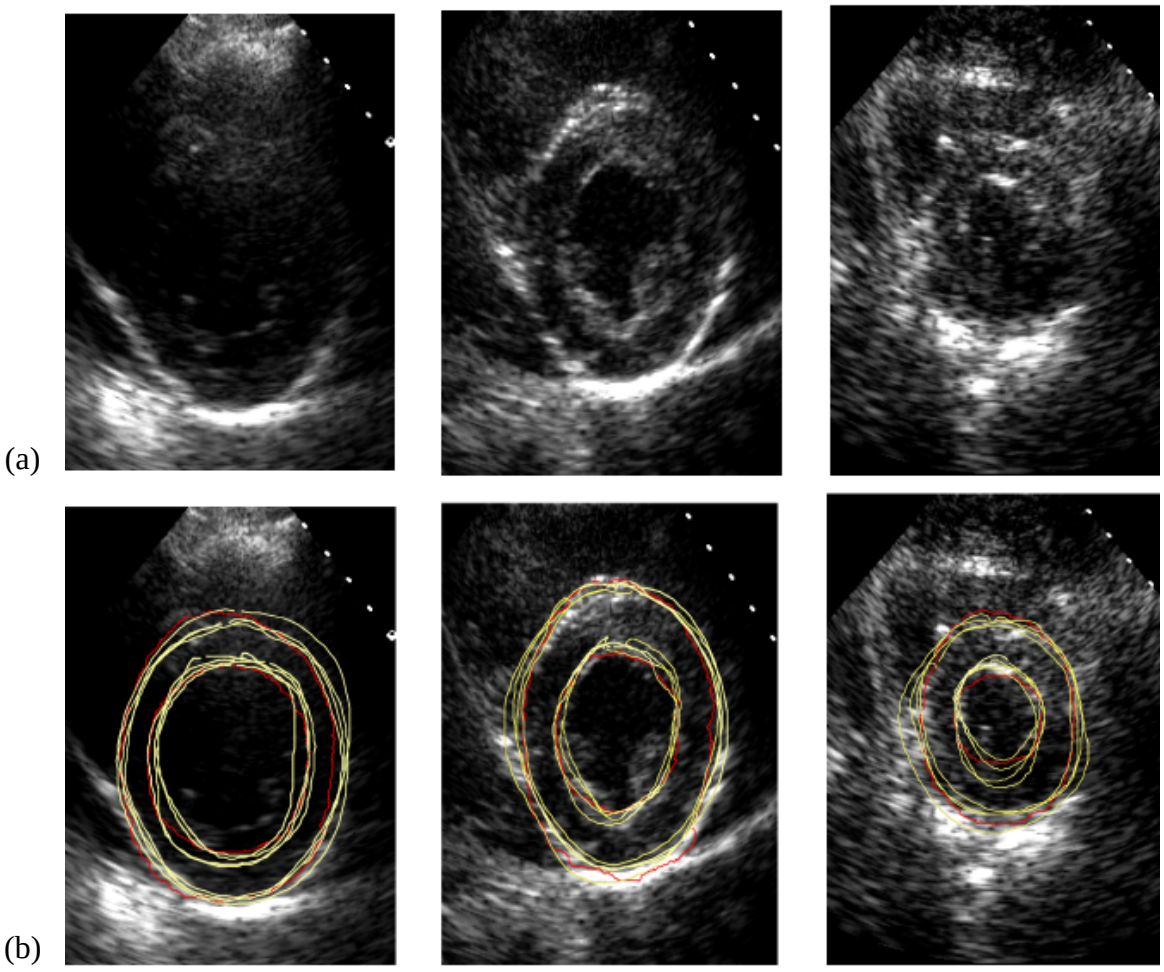

Figure 5 Pixel differences for segmenting an echocardiogram with five different expert contour sets as priors.

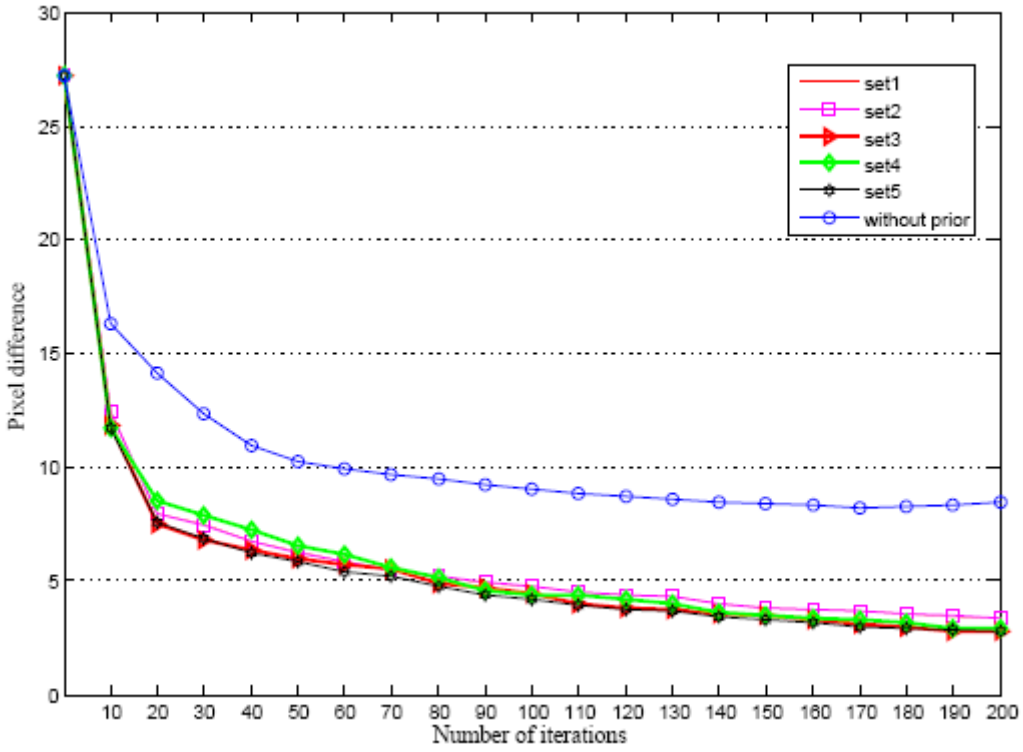

Figure 6 14 cardiac MRIs in the dataset which are cropped for better visualization. An original MRI is shown in Figure 1(b). The red contours are detected by our system and the yellow contours are the expert delineated contours.